Improved Performance of Polymer Solar Cells Featuring One-Dimensional PEDOT Nanorods in a Modified Buffer Layer

Yu-Kai Han,[a,z] **Mei-Ying Chang,**[b] **Wen-Yao Huang,**[b,*] **Hsin-Yu Pan,**[b]
Ko-Shan Ho,[a] **Tar-Hwa Hsieh,**[a] **and Sin-Yu Pan**[b]

[a]*Department of Chemical and Materials Engineering, National Kaohsiung University of Applied Sciences, Kaohsiung 807, Taiwan*
[b]*Department of Photonics, National Sun Yat-Sen University, Kaohsiung 804, Taiwan*

This paper describes the use of one-dimensional (1D) poly(3,4-ethylenedioxythiophene) nanorod (n-PEDOT) and modified poly(3,4-ethylenedioxythiophene):poly(styrene sulfonate) (PEDOT:PSS) films as anode buffer layers in polymer photovoltaic cells based on poly(3-hexylthiophene):[6,6]-phenyl-C_{61}-butyric acid methyl ester. We employed high-speed vibrational milling to disperse the n-PEDOTs into an aqueous PSS medium. Raman spectroscopy measurements revealed quinoid-dominated structures for these aqueous-soluble n-PEDOT:PSS materials. The presence of the 1D n-PEDOTs in the buffer layer improved the photovoltaic performance ($\eta_{AM1.5}$ = 3.10%) of the polymer solar cell relative to that of the system prepared using the unmodified PEDOT:PSS ($\eta_{AM1.5}$ = 2.17%). This enhancement was accompanied by an increase in the values of J_{SC} (from 5.85 to 7.62 mA/cm^2) and the fill factor (from 0.58 to 0.64). The conductivity and polarity of the n-PEDOT–modified buffer layer increased upon increasing the content of n-PEDOT, resulting in increases of the short-circuit current, open-circuit voltage, and power conversion efficiency of the polymer solar cell incorporating the 1D n-PEDOTs.
© 2011 The Electrochemical Society. [DOI: 10.1149/1.3534201] All rights reserved.

Polymer solar cells are attracting much research interest for their application as possible sources of electrical energy because of their attractive combination of flexibility and low-cost fabrication. Many research groups have developed solar cells based on poly(3-hexylthiophene) (P3HT) and conjugated-fullerene composites.[1-6] Although a great progress has been made, with several reported polymer solar cell devices providing power conversion efficiencies (PCEs) of 3–6%, there remains much room for improvement.

The injection ability of a charge transporting material depends critically on the nature of its interfaces with the electrodes. If the injection barrier at the electrodes decreases, the contact resistance will decrease accordingly. On the anode side, the injection barrier decreases when the work function of indium tin oxide (ITO) is increased—for example, through plasma treatment. Poly(3,4-ethylenedioxythiophene) (PEDOT):poly(styrene sulfonate) (PSS) layers, which have work functions higher than that of ITO, have been used as anode buffer layers to increase the performance of several organic solar cells.[7,8] The conductivity of PEDOT:PSS can be increased through the addition of small amounts of glycerol or sorbitol.[9,10] The surface sheet resistance of a PEDOT:PSS film decreases when it is fabricated with the addition of glycerol; however, its optical transparency remains constant.[11] These highly transparent and conductive polymers are ideal candidates for use as anode buffer layers in display devices such as organic light-emitting diodes (OLEDs) or organic solar cells. Kim et al.[12] improved the device performance, including the external electroluminescence quantum efficiency and the current–voltage (*I-V*) luminance characteristics, of an OLED fabricated using a highly conductive and transparent PEDOT:PSS doped with glycerol as an anode buffer layer. Fung et al.[13] fabricated a glycerol-modified PEDOT:PSS anode buffer layer in a polymer light-emitting device (PLED) using poly(9,9-dioctylfluorene) (F8) as the emitter; this glycerol-modified device exhibited a much larger current density relative to that of the unmodified device.

PEDOT:PSS is one of the best hole-conducting buffers because its ionization potential is close to the work function of ITO, whereas its electron affinity (ca. 2.2 eV) is sufficiently low to block electrons.[14] For this reason, the electronic properties of single-wall nanotubes (SWNTs) dispersed in a PEDOT:PSS buffer layer are interesting because pure SWNTs are *p*-type semiconductors.[15,16] These findings encouraged us to study the performance of P3HT:[6,6]-phenyl-C_{61}-butyric acid methyl ester (PCBM)-based polymer solar cells by dispersing PEDOT nanorod (n-PEDOT) materials into PEDOT:PSS buffer layers. Nanostructures of the conducting polymers polypyrrole (PPy) and polyaniline (PANi) have been prepared previously.[17-20] For this study, we chose to use nanostructured PEDOT[21,22] because it possesses several advantageous features: environmental stability, a low redox potential, and a high optical transparency in the doped conducting state.[23]

When used in photovoltaic (PV) devices, PCBM acts as an electron acceptor; it has been intermixed at the nanometer scale with an organic semiconducting polymer (P3HT, electron donor) to obtain a high charge separation yields. Following charge transfer, both electrons and holes must be transported to the electrodes before recombination can occur. In some cases, however, charge transportation is limited by inefficient hopping along poorly formed conduction pathways. Thus, routes that enhance charge transport are desirable to improve the performance of photovoltaic cells. One-dimensional (1D) n-PEDOTs are favorable materials that offer direct pathways for charge transport;[24-27] they can be obtained through chemical synthesis using a hexane/water reverse microemulsion system consisting of sodium bis(2-ethylhexyl) sulfosuccinate (AOT) cylindrical micelles as the template and FeCl$_3$ as the oxidant.[22] The as-synthesized n-PEDOTs are readily dispersed in common organic solvents and films cast on a variety of substrates, but they do not disperse well in aqueous media. Therefore, to disperse the n-PEDOTs into an aqueous medium, we employed the mechanochemical technique of high-speed vibrational milling (HSVM), which had been used previously to prepare organic-soluble, well-ordered 1D SWNTs through the formation of supramolecular complexes.[28] The approach we adapted in this study is superior to that of conventional sonication for preparing water-dispersed n-PEDOT:PSS blends.
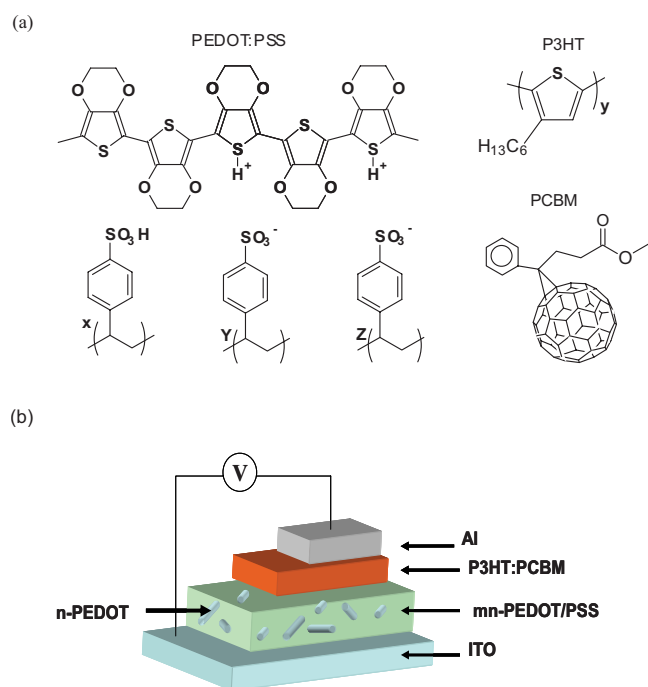
Furthermore, we fabricated polymer solar cells, with and without n-PEDOT modification of the PEDOT:PSS anode buffer layer, in the configuration ITO/PEDOT:PSS/P3HT:PCBM/Al. We constructed the various modified anode buffer layers by adding different amounts of 1D n-PEDOT into a commercialized PEDOT:PSS (Baytron AI 4083) buffer layer (hereafter referred to as mn-PEDOT:PSS).

Experimental

The film thickness was measured using a Dektak 6M stylus profilometer. The optical spectra were measured using a UV/visible spectrophotometer; the work functions of the films were measured using a Riken Keiki AC-2 surface-analyzer photoelectron spectrom-

* Electrochemical Society Active Member.
z E-mail: ykhan@cc.kuas.edu.tw

Scheme 1. (Color online) (a) Chemical structures of the materials used in this study. (b) Architecture of the ITO/n-PEDOT:PSS/P3HT:PCBM/Al heterojunction photovoltaic cell developed in this study.

eter. The surface free energy was determined using a Krüss DSA100 digital surface tension analyzer; three solvents having diversely differing polarities (methylene iodide, water, and glycerol) were used to measure the contact angles of the buffer layer surface. Illumination with white light (100 mW/cm^2) from a Steuernagel solar simulator was used to measure the cell characteristics under AM1.5 conditions. The *I-V* characteristics were recorded using a Keithley 2400 source-meter while illuminating the devices with white light (100 mW/cm^2) from a halogen lamp. The surface morphologies of the films were characterized using a BenYuan CSPM4000 scanning probe microscope and an atomic force microscope operated in the tapping mode. A single-crystalline silicon solar cell was used as a reference cell to confirm the stability of the light source. The mismatch factor was not taken into account. Raman spectra were recorded using a 532-nm diode solid state pumping laser (DSSP) over the scanning range from 400 to 2000 cm^{-1}.

Synthesis of n-PEDOTs.— A reverse microemulsion was first prepared by dissolving AOT (15 mmol) in *n*-hexane (50 mL) and then adding an aqueous solution of FeCl$_3$ (20.0 mmol, 1.0 mL). The resulting orange-colored mixture was stirred gently for 10 min and then EDOT monomer (2 mmol) was added. After 3 h of gentle magnetic stirring, the black precipitate of the n-PEDOTs was suction filtered and washed with a copious amount of methanol.

Modification of buffer layer.— The chemical structures of PEDOT:PSS (Baytron AI4083), P3HT, and PCBM are provided in Scheme 1. Modified buffer layer solutions containing n-PEDOT were prepared by adding n-PEDOT (0.5, 0.1, 0.2, and 0.3 g) into an aqueous PEDOT:PSS solution (10 mL), providing n-PEDOT concentrations of 0.5, 1, 2, and 3 wt %, respectively; vibrating ball-milling was employed to mix these mixtures. The cell containing n-PEDOT and the Baytron mixtures was vibrated in a Retsch MM301 ball-miller five times (40 min for each interval) to obtain a well-dispersed state. Precipitates were observed when the n-PEDOT concentration was greater than 4 wt % in the mn-PEDOT:PSS solution, possibly because PEDOT:PSS formed a gel phase that exhib-
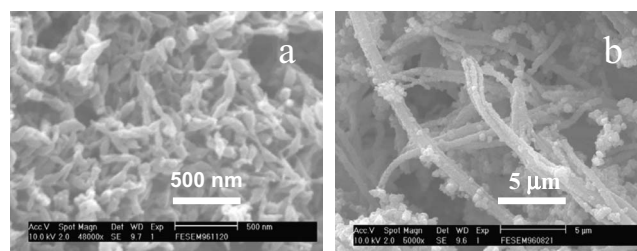

Figure 1. SEM images (a) PEDOT nanorods and (b) PEDOT nanotubes.

ited decreased compatibility with the n-PEDOTs. The conventional PEDOT:PSS and modified mn-PEDOT:PSS layers were prepared through spin-coating onto an ITO glass substrate.

Cell fabrication.— The device configuration of the polymer solar cell is displayed in Scheme 1b. A 60-nm thick mn-PEDOT:PSS or PEDOT:PSS film was prepared through spin-coating onto a UV ozone–treated ITO glass substrate. The sample was dried on a hot plate at $180°$C for 5 min under clean-room conditions. A 50-nm thick layer of the P3HT:PCBM ($1:1$, w/w) blend was then deposited from an *o*-xylene solution. A 200-nm thick aluminum top electrode was deposited under vacuum through a shadow mask.

Results and Discussion

We obtained PEDOT nanorods (Fig. 1a) and nanotubes (Fig. 1b) through emulsion polymerization using various molar ratios of EDOT, FeCl$_3$, and AOT.[22] We found that the PEDOT nanotubes (> 10 µm) did not disperse well in the PSS aqueous media when using the HSVM method, possibly because the PSS polymers could not wrap around the long tubular surfaces of the PEDOT nanotubes to overcome the electrostatic forces holding them together. A more detailed study of the mechanism and greater efforts at dispersing PEDOT nanotubes into aqueous media are currently under investigation.

The n-PEDOTs were quite soluble in the organic solvents dimethylformamide (DMF) and toluene, more so than in aqueous media. The first step required us to formulate stable dispersions of n-PEDOTs in aqueous media. We tested various additives for their ability to create stable dispersions of n-PEDOTs in aqueous media, including common aqueous additives [sodium dodecyl benzene sulfonate (SDBS), camphorsulfonic acid (CSA), sodium dodecyl sulfate (SDS)] and polymeric dopants [PSS, PSS copolymerized with maleic anhydride (PSS-*co*-MA),[29-31] poly(vinyl alcohol),[29,30] poly(*N*-vinylpyrrolidone),[29,31] poly(vinyl methyl ether),[32] hydroxypropylcellulose[33]]. When using the HSVM method, we found that dispersions prepared using water-soluble dopants, such as PSS, formed highly stable dispersions that did not precipitate even after a few weeks (Fig. 2). In well-dispersed aqueous n-PEDOT:PSS solutions, PSS wraps around the surface of the n-PEDOTs, thereby dispersing them well in solution.[34] This technique works well when forming stable dispersions of blended n-PEDOT:PSS in aqueous media, without exposing the n-PEDOTs to other treatment conditions or affecting the conduction properties of the nanostructured PEDOTs.

Figure 3 displays UV/visible spectra of the bulk PEDOT, the n-PEDOTs dispersed in DMF (concentration: ca. 2×10^{-3} g/mL), and n-PEDOT:PSS (1 wt %) in aqueous solution. The spectrum of the n-PEDOTs dispersed in DMF features absorptions at 580 and 850 nm, respectively, indicating that the n-PEDOTs adopted the form of supramolecular complexes, with a longer π–π conjugation and a greater interchain overlap than that of the bulk PEDOT. An interesting feature of the n-PEDOT:PSS absorption is the extended free carrier tail absorption in the near-IR region, suggesting that the extended conjugation length of the n-PEDOT:PSS might provide a longer pathway, relative to that of the bulk PEDOT:PSS, via its 1D
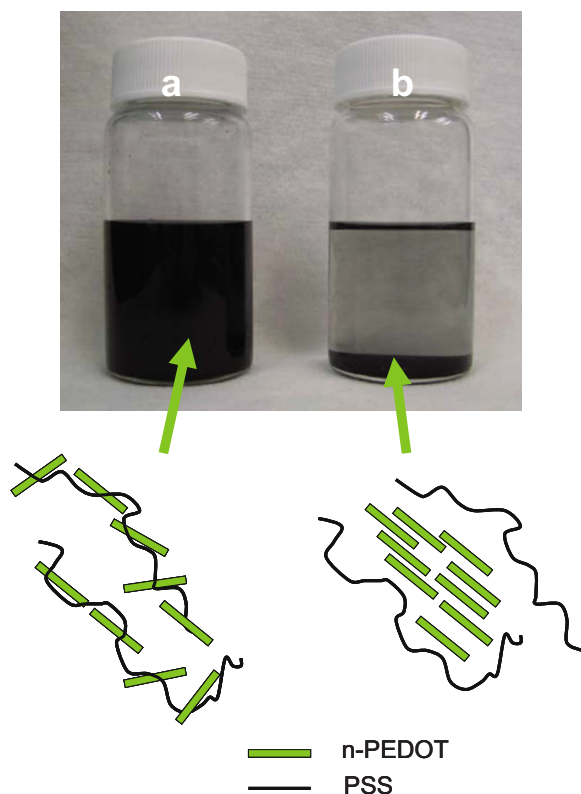
Figure 2. (Color online) Photograph taken 1 week after dispersing n-PEDOT:PSS (1 wt %) in aqueous solutions using (a) HSVM and (b) sonication methods.

Table I. Surface free energies of nmPEDOT:PSS layers.

Composition	Solvent	Θ (°)	Surface free energy (mN/m^2)
PEDOT:PSS	Methylene iodide	31.8	56.17
	Glycerol	47.2	
	Water	44.9	
0.5 wt %	Methylene iodide	32.8	57.34
	Glycerol	45.2	
	Water	42.9	
1 wt %	Methylene iodide	33.9	64.47
	Glycerol	22.8	
	Water	35	
2 wt %	Methylene iodide	35.3	64.95
	Glycerol	19.9	
	Water	34.9	
3 wt %	Methylene iodide	36.5	65.21
	Glycerol	17.5	
	Water	33.7	

fied buffer layer surface from contact angle measurement data obtained using the method described by van Oss.[35-37] The contact angles of water, methylene iodide, and glycerol droplets on the modified surface have been measured to determine the polar and dispersive surface energies of the modified thin films; Table I summarizes the results. Vacca et al.[38] found that the surface energy and polarity of PEDOT:PSS increased upon increasing the PEDOT content. McCandless and co-workers[39] found that higher polar surface energies corresponded to higher-polarity surfaces and provided enhanced crystallization. We observed that the surface energy of the modified buffer layers increased upon increasing the n-PEDOT content; i.e., the surface polarity of the modified buffer layer changed after adding the polar semicrystalline n-PEDOT component. We suspected that (i) the polar surface of this modified mn-PEDOT:PSS buffer layer affected the plane-on or edge-on texture of the P3HT polymeric crystallites and the exciton separation ability at the bulk heterojunction (BHJ) interface[40] and (ii) the change in dipole moment of the buffer layer would help the transportation of holes to the electrode without recombination with electrons, thereby increasing the photovoltaic performance.[41]

Raman spectroscopy is one of the most useful tools for studying the doping behavior of conjugated polymers.[42,43] We used it to confirm the presence of doping phenomena during the formation of n-PEDOT:PSS composites with and without the application of the HSVM method. Figure 4a compares the Raman spectra of blended n-PEDOT:PSS prepared with and without the use of the HSVM method; Fig. 4b presents the benzoid and quinoid resonance structures of PEDOT. We attribute the principle Raman bands at 1267, 1367, 1433, 1449, and 1512 cm^{-1} to $C_\alpha = C_{\alpha'}$ inter-ring stretching,

tubular structure and interchain overlapping, for holes to travel without exciton recombination or interference from impurities.

The surface tension and surface free energy of a film formed through spin-coating or solution processing are important parameters affecting its adhesion (technically significant for its capability to transport carriers from one layer to another), its adhesive bonding, and the adjustment of the hydrophilic and hydrophobic properties of the surface morphology. We derived the surface energy of the modi-
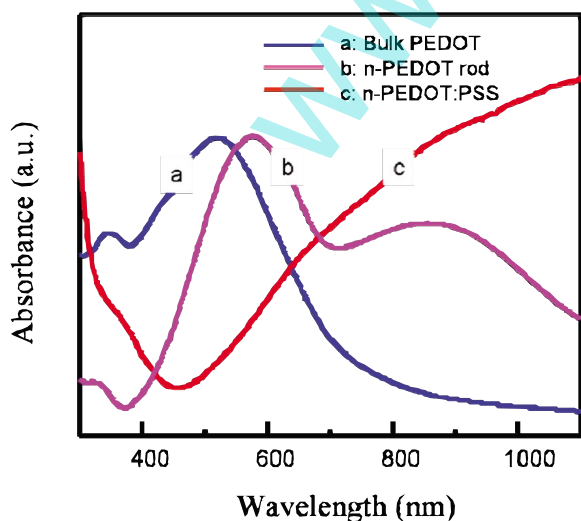

Figure 3. (Color online) UV/visible absorption spectra of the bulk PEDOTs, n-PEDOTs dispersed in DMF, and n-PEDOT:PSS dispersed in aqueous solution.
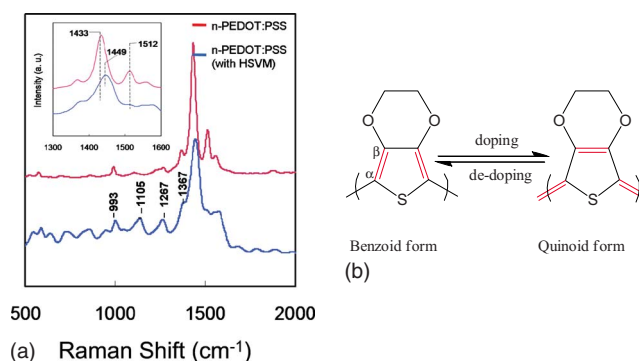

Figure 4. (Color online) (a) Raman spectra of n-PEDOT:PSS samples. (b) Benzoid and quinoid resonance structures.
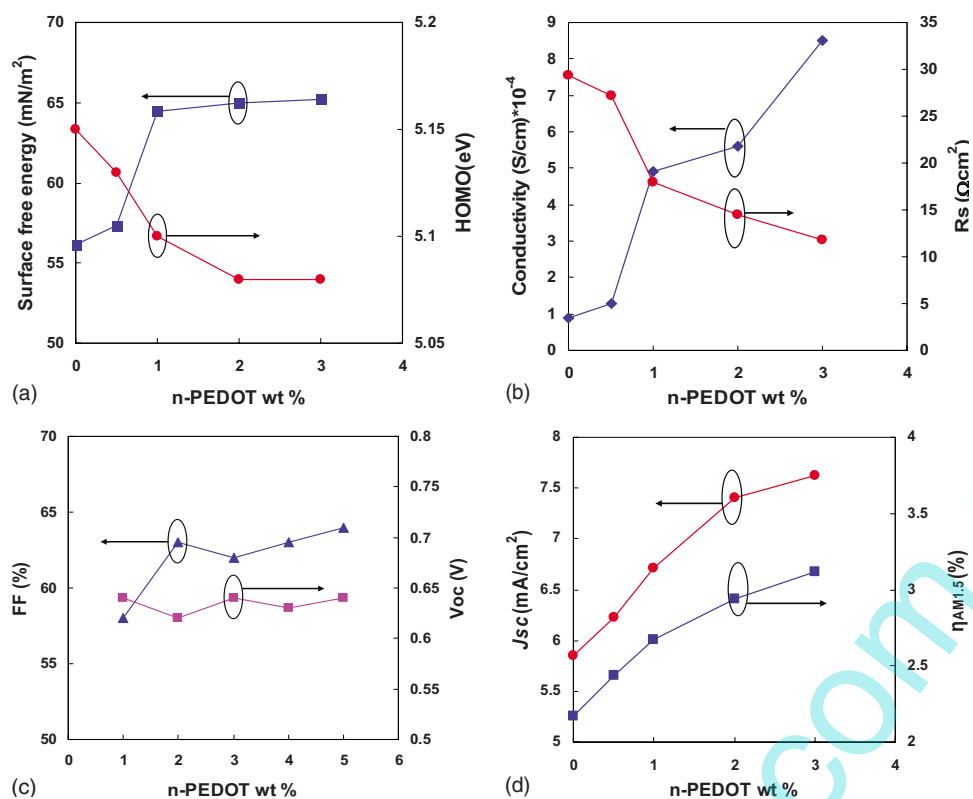
Figure 5. (Color online) (a) Surface free energy and HOMO energy level, (b) series resistance (R_S) and conductivity, (c) open-circuit voltage (V_{OC}) and fill factor (FF), (d) short-circuit current (J_{SC}) and PCE ($\eta_{AM1.5}$), plotted with respect to the weight percentage content of n-PEDOTs.

C_β–C_β stretching, symmetrical $C_\alpha = C_\beta$ stretching, and oxidized symmetrical $C_\alpha = C_\beta$ stretching, and asymmetrical $C_\alpha = C_\beta$ stretching, respectively.[44-47] The intensity of the signal at 1267 cm^{-1} was greater for the n-PEDOT:PSS complexes obtained using the HSVM method, indicating that the oxidative PSS dopants caused the n-PEDOT polymer backbones to adopt predominantly quinoid structures. The intensity of the C_β–C_β stretching band at 1367 cm^{-1} decreased when the PSS dopants were anchored on the n-PEDOT backbones, suggesting a limited C_β–C_β stretching and a favored stabilization of the quinoid structure. The most important shift was that of the symmetrical $C_\alpha = C_\beta$ stretching band, which moved from 1433 to 1449 cm^{-1}, indicating that this vibration was sensitive to oxidizing (doping) and reducing (dedoping) behavior. We attribute this shift to higher wavenumber to shortening of the conjugation length of the neutral polymer backbone upon further oxidation (doping). At low doping levels, the $C_\alpha = C_\beta$ stretching band was dominated by the neutral benzoid structure and, therefore, it appeared closer to 1433 cm^{-1}; it shifted to 1449 cm^{-1} when the doping level was higher. Thus, a transformation of the resonance structure of the n-PEDOT thiophene backbone occurred after doping with PSS. The intensity of the signal for the $C_\alpha = C_\beta$ asymmetric band at 1512 cm^{-1} for the HSVM-prepared n-PEDOT:PSSs was lower than that of the blended n-PEDOT:PSS, indicating that the doped structures featured predominantly in-plane, symmetric, resonance-conjugated backbones.[48]

Thus, using the HSVM approach can provide higher doping levels and aqueous-dispersible n-PEDOT:PSS materials. In addition, this n-PEDOT:PSS material exhibited a conductivity that was ca. 2.9 S/cm higher than that of the commercial PEDOT:PSS material AI 4083 (ca. 10^{-3} S/cm) and a work function of ca. 5.15, making it potentially suitable for use as a good hole transporting material in organic electronics applications.

From AC-2 measurements, we determined the energy levels of the highest occupied molecular orbitals (HOMOs) of the n-PEDOTs and PEDOT:PSS to be ca. 4.9 and ca. 5.15 eV, respectively. Lee and Chung[49] improved the luminous efficiency and work function of a device incorporating a conventional PEDOT:PSS by increasing the

concentration of PSS on the film surface. In this study, we found that the work function of the conventional PEDOT:PSS could be tuned merely by controlling the ratio of n-PEDOT to PEDOT:PSS. The work function of the modified buffer layer decreased from ca. 5.15 to ca. 5.08 eV upon increasing the n-PEDOT concentration from 0 to 3 wt %; i.e., incorporation of n-PEDOT:PSS into PEDOT:PSS had a soft effect on the HOMO energy level [Fig. 5a].

Figure 5 and SM 1 display the *I-V* characteristics of cells incorporating and lacking n-PEDOT:PSS in the buffer layer; Table II summarizes the photovoltaic performance of the cells containing the various mn-PEDOT:PSS anode buffer layers. Figure 5b presents the conductivity–series resistance (R_S) characteristics of the PEDOT:PSS films as a function of the initial concentration of n-PEDOTs. The unmodified PEDOT:PSS film formed through spin-coating of an aqueous solution of Baytron AI 4083 had a conductivity of ca. 8.9×10^{-5} S/cm. This value was enhanced after the addition of n-PEDOT:PSS, presumably because the n-PEDOTs provided longer conducting pathways for carriers in the mn-PEDOT:PSS film and increased the charge-carrier mobility.[13] The maximum conductivity of 8.5×10^{-4} S/cm was obtained after adding 3 wt % n-PEDOT to the unmodified buffer film. The optical transparency of the original buffer layer was retained after modification with 3 wt % n-PEDOT.

We analyzed the photovoltaic characteristics of the devices based on the equivalent circuit; this approach has been used frequently to describe the electric behavior of photovoltaic devices.[6] The current density–voltage characteristics can be described by the dark *i-V* curve and fitted by the standard one-diode model

$$I = I_o \left[\exp\left(\frac{q(V - IR_s)}{nkT}\right) - 1 \right] + \frac{q(V - IR_s)}{R_{SH}} \qquad [1]$$

where I_0 is the saturation current, q is the magnitude of the electronic charge, V is the applied voltage, n is the ideality factor, k is Boltzmann constant, T is the absolute temperature, R_S is the series resistance, R_{SH} is the shunt resistance, and I_{PH} is the photocurrent. The series resistance can be estimated from the inverse slope at a positive voltage where the *I-V* curves become linear; a lower series

Table II. Conductivities and work functions of modified buffer layers.

Sample	Composition	HOMO (eV)	Conductivity[a] (S/cm)	R_S (Ω cm^2)	V_{OC} (V)	J_{SC} (mA/cm^2)	FF	$\eta_{AM1.5}$ (%)
1	PEDOT:PSS	5.15	8.9×10^{-5}	29.4	0.64	5.85	0.58	2.17
2	0.5 wt %	5.13	1.3×10^{-4}	27.2	0.62	6.23	0.63	2.44
3	1 wt %	5.10	4.9×10^{-4}	18.0	0.64	6.71	0.62	2.67
4	2 wt %	5.08	5.6×10^{-4}	14.5	0.63	7.41	0.63	2.94
5	3 wt %	5.08	8.5×10^{-4}	11.8	0.64	7.62	0.64	3.12
6	n-PEDOT	4.90	2–3	—	—	—	—	—

[a] Conductivity of the buffer layer was measured using the technique described on the Heraeus Clevios website.[51]

resistance reveals that a higher current will flow through the device. Table II lists the values of R_S that we obtained from the *I-V* curves of the devices; a significant decrease in R_S occurred when the device incorporated an mn-PEDOT:PSS layer modified with introduced n-PEDOTs. The series resistance, which can be expressed as the sum of the bulk and interfacial resistances, can reflect ohmic loss in solar cells; ohmic loss includes the resistance of the organic/electrode contacts, the photoactive layer, the electrodes, and the parasitic probe resistance.[50] It is likely that the two interfaces featuring the introduced n-PEDOTs (i.e., the ITO/mn-PEDOT:PSS and mn-PEDOT:PSS/active layer interfaces) provided much-lower-magnitude series resistances relative to that of the PEDOT:PSS/active layer contact. The introduction of the 1D n-PEDOTs decreased the series resistance and increased the conductivity of the buffer layer in the device. The fill factor (FF) also increased, from 0.58 to 0.64, upon increasing the conductivity of the buffer layer.

Figure 5c presents plots of the open-circuit voltages (V_{OC}) and FFs with respect to the n-PEDOTs content. The value of V_{OC} of the cells remained relatively constant, in the range ca. 0.62–0.64 V, suggesting an equal energy difference between the HOMO of the donor and the lowest unoccupied molecular orbital (LUMO) of the acceptor in the various systems.

Figure 5d displays the values of J_{SC} and the efficiency characteristics of the devices incorporating effective n-PEDOT contents ranging from 0 to 3 wt %. The values of J_{SC} are highly dependent on the conductivity of the buffer layer, increasing from 5.85 to 7.62 mA/cm^2 when the buffer layer conductivity increased from 8.9×10^{-5} to 8.5×10^{-4} S/cm; in contrast, the value of V_{OC} remained relatively constant (ca. 0.64 V).

Incorporating a suitable amount of n-PEODTs into the buffer layer increased the film's conductivity from 8.9×10^{-5} to 8.5 $\times 10^{-4}$ S/cm. The increased carrier transport enhanced the short-circuit current density of the devices; likewise, the increased short-circuit current density and FF enhanced the PCE. As a result, the maximum PCE of the cell (3.10%) occurred when the n-PEDOT

concentration was 3 wt %; the corresponding values of J_{SC}, V_{OC}, and FF were 7.62 mA/cm^2, 0.64V, and 0.65, respectively. The PCE increased from ca. 2.17 to ca. 3.10% after incorporating the 1D PEDOT nanorods into the buffer layer, thereby increasing the PV cell characteristics.

Scheme 2 depicts our proposed mechanism for carrier transport through the modified buffer layer: (i) The BHJ photoactive layer generates excitons after accepting photons from the sunlight illuminator. (ii) The internal electric field separates the excitons at the BHJ interfaces and causes them to be swept to their respective electrodes. (iii) The photoinduced holes hop into the nanoscale interface between the mn-PEDOT:PSS and the active layer and are swept into the modified buffer layer. (iv) The partial photogenerated holes cross the buffer layer via the high-conductivity n-PEDOT pathways surrounding the PDEOT:PSS conductive amorphous phase, decreasing the degrees of interference from impurities and recombination with electrons. (v) The surviving holes and electrons pass through the energy barriers of the ITO and Al films to generate the electric current.

Conclusion

We have fabricated a polymer solar cell incorporating n-PEDOT–modified mn-PEDOT:PSS as the anode buffer layer. Relative to the polymer solar cell prepared using unmodified PEDOT:PSS ($\eta_{AM1.5}$ = 2.17%), the presence of the 1D n-PEDOTs improved the PCE ($\eta_{AM1.5}$ = 3.10%). This enhancement was accompanied by an increase in the values of J_{SC} (from 5.85 to 7.62 mA/cm^2) and the FF (from 0.58 to 0.64). This superior device performance arose from the increased conductivity and polarity of the n-PEDOT–modified buffer layer, which provided more-efficient pathways for holes than those in the more frequently used PEDOT:PSS buffer layers. As a result, the hole collection barrier height was reduced, and the photovoltaic response was improved.
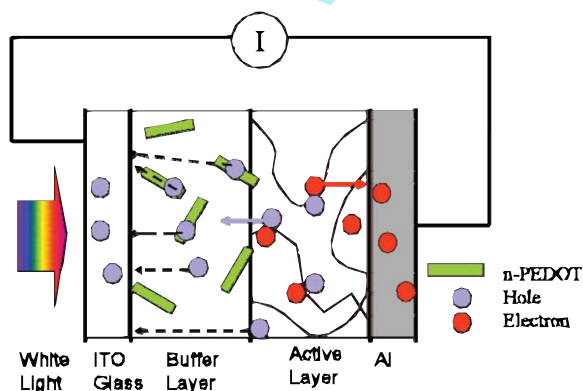
Scheme 2. (Color online) Cartoon representation of the carrier transporting mechanism in the photovoltaic cell under illumination with white light.

References

1. G. Yu, J. Gao, J. C. Hummelen, F. Wudl, and A. J. Heeger, *Science*, **270**, 1789 (1995).
2. S. E. Shaheen, C. J. Brabec, N. S. Sariciftci, F. Padinger, T. Fromherz, and J. C. Hummelen, *Appl. Phys. Lett.*, **78**, 841 (2001).
3. M. Svensson, F. Zhang, S. C. Veenstra, W. J. H. Verhees, J. C. Hummelen, J. M. Kroon, O. Inganas, and M. R. Andersson, *Adv. Mater.*, **15**, 988 (2003).
4. F. Padinger, R. S. Rittberger, and N. S. Sariciftci, *Adv. Funct. Mater.*, **11**, 1 (2003).
5. M. A. Ibrahim, O. Ambacher, S. Sensfuss, and G. Gobsch, *Appl. Phys. Lett.*, **86**, 201120 (2005).
6. W. Ma, C. Yang, X. Gong, K. Lee, and A. J. Heeger, *Adv. Funct. Mater.*, **15**, 1617 (2005).
7. C. J. Brabec, N. S. Sariciftci, and J. C. Hummelen, *Adv. Funct. Mater.*, **11**, 15 (2001).
8. P. Peumanns and S. R. Forrest, *Appl. Phys. Lett.*, **79**, 126 (2001).
9. T. Granlund, L. A. A. Pettersson, and O. Inganas, *J. Appl. Phys.*, **89**, 5897 (2001).
10. S. Ghosh and O. Inganas, *Synth. Met.*, **121**, 1321 (2001).

11. A. J. Makinen, I. G. Hill, R. Shashidhar, N. Nikolov, and Z. H. Kafafi, *Appl. Phys. Lett.*, **79**, 557 (2001).
12. W. H. Kim, A. J. Makinen, N. Nikolov, R. Shashidhar, H. Kim, and Z. H. Kafafi, *Appl. Phys. Lett.*, **80**, 3844 (2002).
13. M. K. Fung, S. L. Lai, S. W. Tong, M. Y. Chan, C. S. Lee, and S. T. Lee, *Appl. Phys. Lett.*, **81**, 1497 (2002).
14. M. Baibarac and P. Gomez-Romero, *J. Nanosci. Nanotechnol.*, **6**, 1 (2006).
15. R. D. Antonov and A. T. Johnson, *Phys. Rev. Lett.*, **83**, 3274 (1999).
16. H. S. Woo, R. Czerw, S. Webster, D. L. Carroll, J. W. Park, and J. H. Lee, *Synth. Met.*, **116**, 369 (2001).
17. J. Jang and H. Yoon, *Chem. Commun. (Cambridge)*, **6**, 720 (2003).
18. M. Delvaux, J. Duchet, P. Y. Stavaux, R. Legras, and S. Demoustier-Champagne, *Synth. Met.*, **113**, 275 (2000).
19. S. Demoustier-Champagne and P. Y. Stavaux, *Chem. Mater.*, **11**, 829 (1999).
20. Q. Pei, G. Zuccarello, M. Ahlskog, and O. Inganas, *Polymer*, **35**, 1347 (1994).
21. J. Jang, M. Chang, and H. Yoon, *Adv. Mater.*, **17**, 1616 (2005).
22. X. Zhang, J. S. Lee, G. S. Lee, D. K. Cha, M. J. Kim, D. J. Yang, and S. K. Manohar, *Macromolecules*, **39**, 470 (2006).
23. Y. H. Ha, N. Nikolov, S. K. Pollack, J. Mastrangelo, B. D. Martin, and R. Shashidhar, *Adv. Funct. Mater.*, **14**, 615 (2004).
24. W. U. Huynh, J. J. Dittmer, and A. P. Alivisatos, *Science*, **295**, 2425 (2002).
25. W. U. Huynh, J. J. Dittmer, W. C. Libby, G. L. Whiting, and A. P. Alivisatos, *Adv. Funct. Mater.*, **13**, 73 (2003).
26. B. Sun, E. Marx, and N. C. Greenham, *Nano Lett.*, **3**, 961 (2003).
27. J. Jiu, S. Isoda, F. Wang, and M. Adachi, *J. Phys. Chem. B*, **110**, 2087 (2006).
28. K. Komatsu, K. Fujiwara, Y. Murata, and T. Braun, *J. Chem. Soc., Perkin Trans. 1*, **1**, 2963 (1999).
29. J. Stejskal and P. Kratochvil, *Langmuir*, **12**, 3389 (1996).
30. P. Ghosh, S. K. Siddhandta, S. R. Haque, and A. Chakrabarti, *Synth. Met.*, **123**, 83 (2001).
31. T. Sulimenko, J. Stejskal, I. Krivka, and J. Prokes, *Eur. Polym. J.*, **37**, 219 (2001).
32. B. D. Chin and O. O. Park, *J. Colloid Interface Sci.*, **234**, 344 (2001).
33. J. Stejskal, M. Spikova, A. Riede, M. Helmstedt, P. Mokreva, and J. Prokes, *Polymer*, **40**, 2487 (1999).
34. M. J. O'Connell, P. Boul, L. M. Ericson, C. Huffman, Y. H. Wang, E. Haroz, C. Kuper, J. Tour, K. D. Ausman, and R. E. Smalley, *Chem. Phys. Lett.*, **342**, 265 (2001).
35. C. J. van Oss, R. J. Good, and M. K. Chaudhury, *Adv. Colloid Interface Sci.*, **28**, 35 (1987).
36. C. J. van Oss, R. J. Good, and M. K. Chaudhury, *J. Chromatogr.*, **53**, 191 (1987).
37. C. J. van Oss, R. J. Good, and M. K. Chaudhury, *Langmuir*, **4**, 884 (1988).
38. P. Vacca, M. Petrosino, R. Miscioscia, G. Nenna, C. Minarini, D. Della Sala, and A. Rubino, *Thin Solid Films*, **516**, 4232 (2008).
39. M. S. Angelo, B. E. McCandless, R. W. Birkmire, S. A. Rykov, and J. G. Chen, *Prog. Photovoltaics*, **15**, 93 (2007).
40. A. Salleo, *Mater. Today*, **38**, 10 (2007).
41. H. Ishii, K. Sugiyama, E. Ito, and K. Seki, *Adv. Funct. Mater.*, **11**, 972 (1999).
42. S. Lefrant, E. Mulazzi, E. Faulques, and E. Perrin, *J. Mol. Electron.*, **4**, 167 (1988).
43. S. Lefrant, J. P. Buisson, and H. Eckhardt, *Synth. Met.*, **37**, 91 (1990).
44. S. Garreau, G. Louarn, J. P. Buisson, G. Froyer, and S. Lefrant, *Macromolecules*, **32**, 6807 (1999).
45. Y. Furukawa, *J. Phys. Chem.*, **100**, 15644 (1996).
46. N. Sakmeche, J. J. Aaron, M. Fall, S. Aeiyach, M. Jouini, J. C. Lacroix, and P. C. Lacaze, *Chem. Commun. (Cambridge)*, **24**, 2723 (1996).
47. W. W. Chiu, J. Travaš-Sejdic, R. P. Cooney, and G. A. Bowmaker, *Synth. Met.*, **155**, 80 (2005).
48. N. R. Chiou and A. J. Epstein, *Adv. Mater.*, **17**, 1679 (2005).
49. T. W. Lee and Y. S. Chung, *Adv. Funct. Mater.*, **18**, 2246 (2008).
50. G. Xue, S. Uchida, B. P. Rand, and S. R. Forrest, *Appl. Phys. Lett.*, **84**, 3013 (2004).
51. Heraeus Clevios, http://www.clevios.com/index.php?page_id=1178, last accessed Jan 9, 2011.